VALIDATION OF THE THEORETICAL APPROACH FOR MODELLING OF THE HYDRIDE MORPHOLOGY WITH EXPERIMENTAL DATA OBTAINED FROM SPIZWURZ BUNDLE TEST

Mikhail Kolesnik*, Juri Stuckert, Mirco Grosse, Sarah Weick
Institute for Applied Materials – Applied Materials Physics (IAM-AWP), Karlsruhe Institute of Technology, Karlsruhe, Germany
mikhail.kolesnik@kit.edu

ABSTRACT

This paper presents the calibration and assessment of two complementary simulation tools using new experimental data on hydride morphology in zirconium alloy fuel cladding. The first tool is based on the numerical solution of a system of ordinary differential equations, predicting averaged microstructural quantities including the radial hydride fraction, hydride length and hydride volume density. The second, MORPHYD explicitly simulates the nucleation and diffusion-controlled growth of disc-shaped hydrides within a virtual 3D domain. In the present work, MORPHYD is applied only to 100 wppm cases because its current version is limited to precipitation-only simulations of small, non-overlapping hydrides. MORPHYD also enables the evaluation of hydride network connectivity metrics and their statistical distributions based on the Monte Carlo method, repeating the simulations a statistically significant number of times. In both approaches, hydride nucleation is described within a classical heterogeneous framework in which the defect energy for nucleation sites is defined by the user-specified distribution. Both modelling approaches were calibrated using new experimental data obtained from the SPIZWURZ bundle test on cladding tubes manufactured from Zircaloy-4 and opt. ZIRLO. The SPIZWURZ included long-term hydride reorientation experiments conducted at the LICAS facility of the Karlsruhe Institute of Technology. The test bundle consisted of 21 hydrogen-charged cladding tubes, each 2.5 meters long, which were subjected to slow, stepwise cooling over 250 days to reproduce as close as possible dry storage conditions for spent nuclear fuel. The following morphological parameters were measured experimentally across a spectrum of hydrogen concentrations and applied stresses: radial hydride fraction, hydride length and surface density, hydride continuity coefficient (HCC) and radial hydride continuity path (RHCP). The results show that, after calibration, both simulation tools reproduce the main experimental trends in hydride morphology and connectivity, supporting their further development and application for assessing hydride embrittlement of fuel rod cladding under dry storage conditions.

KEYWORDS
hydride embrittlement, zirconium alloys, dry storage, spent nuclear fuel, modelling

1. INTRODUCTION

Hydride embrittlement of zirconium claddings can pose a risk to the integrity of cladding tubes, especially during post-operational storage [1], [2]. Hydrides are capable of providing low energy brittle crack pathways, which determine the influence of hydride morphology on the degree of embrittlement [3]. Macroscale hydride morphology is the result of the agglomeration (or stacks) of microscale ones, forming a complex "cornflake" 3D surface [4], [5]. In simplified form, macroscale hydrides can be approximated as plates and specified by their length, thickness, volume density and orientation. The entire hydride network can also be characterized by its connectivity. Hydride connectivity shows the strongest correlation with the

degree of hydride embrittlement among other metrics [6]. The ductile to brittle transition is associated with percolation of brittle crack through hydrides and corresponds to the threshold of the connectivity [3].

The morphology of hydrides is determined by the alloy texture, hydrogen concentration and thermomechanical conditions during hydride precipitation and growth. The orientation of hydrides at low stresses is determined by the texture and microstructure of the alloy. However, when external stresses exceed the threshold, hydrides tend to nucleate and grow perpendicular to the external tension [7]. Temperature is another parameter that can theoretically influence the orientation of precipitating hydrides [8]. The density, length and thickness of the hydrides are strongly determined by the cooling rate. Slow cooling rates increase length and thickness and decrease number density [9].

Temperature regimes for long-term dry storage (DS) and transport of spent nuclear fuel (SNF) include the drying of fuel assemblies in storage or transport casks. During drying, the temperature of the fuel assemblies can rise to about ~ 400 °C due to decay heat in the fuel pellets, resulting in dissolution of all or a significant part of the hydrides. The hydrides will later reprecipitate as the temperature slowly decreases with the natural reduction of decay power. Meanwhile, the cladding is loaded by the internal gas pressure, creating hoop tension. These conditions can potentially lead to the precipitation of long radially oriented hydrides, increasing the degree of embrittlement. The safety assessment of DS regimes should include the prediction of hydride morphology, based on experimental investigations of embrittlement mechanisms and simulations adapted to particular conditions. Research in both directions is currently being carried out at the Karlsruhe Institute of Technology (KIT) within the framework of the SPIZWURZ project [10]. This paper presents the results of the calibration of two theoretical approaches developed for the simulation of hydride morphology in zirconium alloys on new experimental data.

2. EXPERIMENTAL CONDITIONS. SPIZWIRZ BUNDLE TEST

The experimental SPIZWURZ bundle consisted of 21 cladding tubes with a length of 2.5 m, manufactured from Zircaloy-4, opt. ZIRLO, and the duplex alloy DX-D4 and hydrogen-charged to one of two target concentrations, 100 or 300 wppm. The spatial arrangement of the rods within the bundle is shown in Fig. 1. A detailed analysis of the experimental results concerning hydride morphology, as well as a description of the SPIZWURZ experiment, can be found in [11].

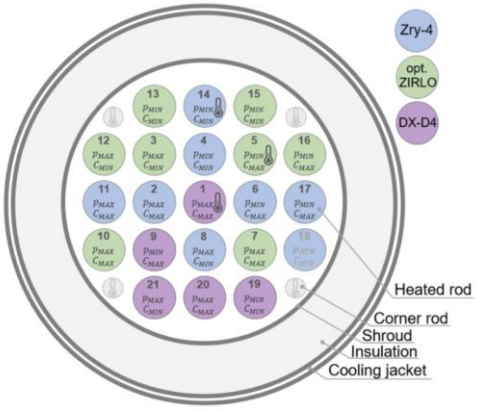

Figure 1: Schematic cross-section of the SPIZWURZ bundle. Rod arrangement

At the present stage, eight rods were selected for simulation and comparison with experimental data. These included rods 2, 4, 6, and 8 manufactured from Zircaloy-4 and rods 10, 12, 15, and 16 manufactured from opt. ZIRLO. For each alloy, the selected rods represent all combinations of the two target hydrogen

concentrations and two target internal gas pressure levels. The internal gas pressure histories applied in the simulated rods are shown in Fig. 2. Two target pressure levels, 106 and 146 bar, corresponding to approximate hoop stresses of 68 and 93 MPa, respectively.

The thermal scenario of the bundle consisted of heating up to approximately 400 °C, followed by slow, stepwise cooling. The axial temperature profiles measured by thermocouples in three instrumented rods are shown in Fig. 3*a*, where the axial coordinate of 0 mm corresponds to the beginning of the actively heated region. Fig. 3*b* presents the temperature history in the hottest axial position of rod 1 (at an elevation of 520 mm). Several abrupt temperature drops (Fig. 3*b*) are associated with unexpected power blackouts during the experiment. For the numerical simulations, smoothed temperature histories were applied, Fig. 3*b*.

The rods selected for simulations were not equipped with thermocouples; therefore, their temperature histories had to be inferred. Rods 2, 4, 6, and 8 are located symmetrically in the second layer of the bundle. Consequently, their temperature scenarios were assumed to be identical and were defined as the average of the thermocouple readings from rods 1 and 5. Rods 10, 12, 15, and 16 are located in the outer layer of the bundle; for these rods, the temperature histories were assumed to be identical to each other and equal to the thermocouple measurements obtained from rod 14, which belongs to the same layer. All temperature scenarios assumed in the simulations were smoothed in a similar way to that shown in Fig. 3*b* for the hottest zone of rod 1. These smoothed profiles remove abrupt temperature drops, short-term fluctuations of about 5 °C during holding periods, and minor non-monotonic variations, while preserving the overall thermal history and the effective cooling rates of the main cooling steps for calibration and assessment.

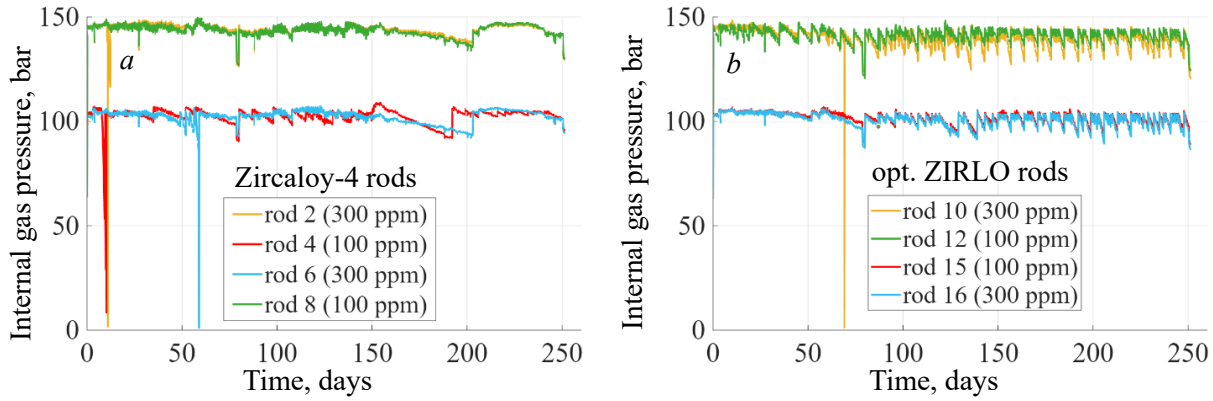

Figure 2. Internal pressure scenarios in simulated rods: a) – Zircaloy-4 rods, b) – opt. ZIRLO rods

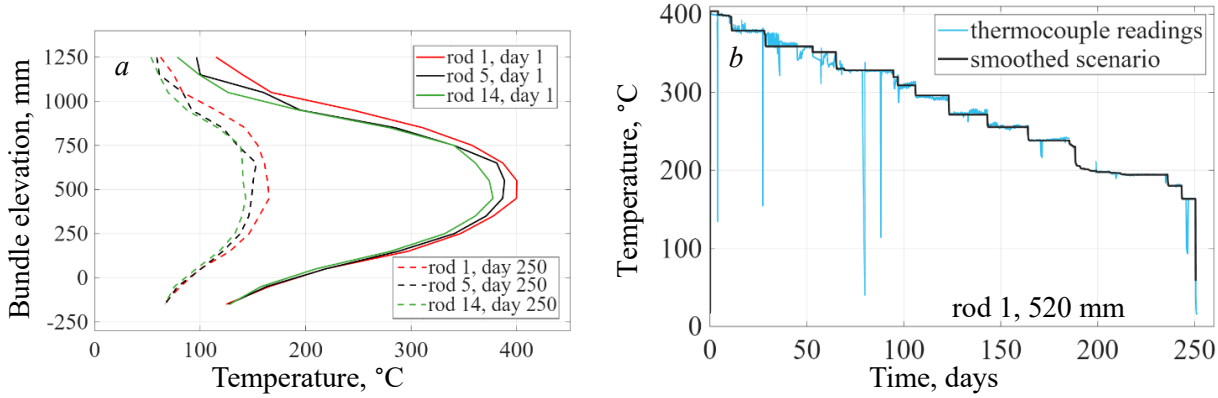

Figure 3. Bundle temperature: a) axial temperature profiles, b) temperature scenario in rod 1 at 520 mm: thermocouple readings and smoothed temperature scenario, used in simulations

3. A SIMULATION TOOL BASED ON ODE SYSTEM SOLUTION

3.1. The description of the tool

The first approach is based on the numerical solution of the system of ordinary differential equations (ODE). The simulation tool used here is based on the concept described in [12] after modernization. The ODE system has four independent variables: the hydrogen concentration in solid solution (C_s), the fraction of hydrides elongated in the radial direction (θ) and the volume density of the radial and circumferential hydrides (n_r and n_r).

The kinetics of hydrogen concentration in solid solution C_s during dissolution and precipitation of hydrides is described as the relaxation of supersaturation with a characteristic time τ_0, by analogy with [13]:

$$\frac{\mathrm{d}C_s}{\mathrm{d}t} - \frac{C_s - C_e}{\tau_0} = 0 \tag{1}$$

where C_e denotes the equilibrium hydrogen solubility, which is different for dissolution and precipitation; the characteristic time τ_0 is estimated as $\tau_0 = V_{per\ hydride}/(d \cdot D_{\mathrm{H}})$, where $V_{per\ hydride} = n^{-1}$ is the volume per hydride (n is the mean hydride concentration), and dD_{H} characterizes the diffusional-controlled sink efficiency of an average hydride, with d being the average hydride diameter and D_{H} the hydrogen diffusion coefficient.

The fraction of radially oriented hydrides θ is assumed to be constant during dissolution of hydrides and can be written as follows for precipitation [12], [13]:

$$\frac{\mathrm{d}\theta}{\mathrm{d}t} = -\frac{f_r - \theta}{C_{tot} - C_s} \cdot \frac{\mathrm{d}C_s}{\mathrm{d}t} \tag{2}$$

where C_{tot} is the total hydrogen concentration (both in solid solution and in hydride phase), and f_r is the fraction of hydrogen precipitating as a component of radially oriented hydrides at the current step [12], [13]:

$$f_r = \frac{1}{1 + f_0 \cdot \exp(-\sigma \cdot \Delta\Omega/kT)} \tag{3}$$

where f_0 and $\Delta\Omega$ are model parameters, determined the susceptibility of hydrides to reorientation.

The process of nucleation of new hydrideы on crystal lattice defects is simulated in the classical heterogeneous approximation, where the nucleation rate R is [12]:

$$R = n_0 Z j^* \cdot \exp(-\Delta G^*/kT) \tag{4}$$

where n_0 is the volume density of the nucleation sites, j^* is the hydrogen flow to the critical nucleus of the hydrides, Z is the Zeldovich factor and ΔG^* is the Gibbs energy change after the hydride nucleation, which can be written as [12]:

$$\Delta G^* = \Omega^*(g_m - \Delta\mu/v_{\mathrm{H}}) + S^*\gamma - E_d \tag{5}$$

where g_m is the mechanical deformation energy due to the volume dilatation [12], $\Delta\mu$ is the chemical energy change per unit volume, v_{H} is the atomic volume of hydrogen, γ is the metal/hydride interphase energy, Ω^* and S^* are the volume and surface area of the critical hydride nucleus, E_d is the defect energy of the nucleation sites. The defect energy of the particular nucleation site depends on the defect type and its specific features and is assumed here to be a random value with a normal distribution. The nucleation kinetics of hydride stacks at the precipitation stage is estimated as the integral over all vacant nucleation sites of the nucleation frequency from Eq. (4), [12]:

$$\frac{\mathrm{d}n}{\mathrm{d}t} = \int_{E_{d,min}}^{E_{d,max}^{frei}} Gauss(E_d) \cdot R(E_d) \cdot \mathrm{d}E_d \tag{6}$$

Gauss denotes a normal distribution over energies, with the mean value E_{d0} and standard deviation $\bar{\sigma}$. Nucleated hydrides are radial with probability equal to f_r and circumferential with probability $(1 - f_r)$:

$$\frac{\mathrm{d}n_r}{\mathrm{d}t} = f_r \cdot \mathrm{d}n, \quad \text{and} \quad \frac{\mathrm{d}n_c}{\mathrm{d}t} = (1 - f_r) \cdot \mathrm{d}n \tag{7}$$

It is assumed, that the nucleation sites with maximum defect energy are filled first, and therefore the maximum defect energy of vacant nucleation sites $E_{d,max}^{frei}$, required for the integration in Eq. (6), is [12]:

$$\frac{1 + \mathrm{erf}\left(\left(E_{d,max}^{frei}, -E_{d0}\right)/\sqrt{2} \cdot \bar{\sigma}\right)}{2} = \frac{n_r + n_c}{n} \tag{8}$$

The ODE system, including Eqs. (1), (2) and (7), is solved numerically. The main model parameters are presented in Table I in the Appendix.

3.2. Calibration and assessment of the approach based on the ODE solution

Fig. 4 present the comparison of calculated RHF on experimental data for Zircaloy-4. Two sets of numerical results are shown: blind pre-test and post-test simulations. The pre-test simulations systematically overestimate the RHF, whereas the post-test simulations exhibit significantly improved agreement with the experimental data. This discrepancy can be attributed to two main factors. First, the actual hydrogen concentrations were determined only after the experiments by destructive hot-gas extraction, which data were not available for pre-test simulations. Second, different parameter sets governing hydride reorientation (f_0 and $\Delta\Omega$ in Eq. (3)) were used in the pre-test and post-test simulations. In the pre-test simulations, these parameters were fitted using the most conservative values reported in the literature (Fig. 8*a* in [14]), which resulted in an over-conservative prediction of RHF. For the post-test simulations, the model parameters were calibrated using a larger experimental database, including the new results obtained within the SPIZWURZ experiment, leading to a substantially improved model–experiment agreement. Since SPIZWURZ data were included in calibration, these post-test simulations are used to assess calibrated model performance and identify remaining deviations and trends, rather than as fully independent validation. A noticeable deviation is seen only for rod 8. We attribute this to a likely contact between the cladding and the pellet imitator, which is supported by the abnormal deformation pattern of this tube.

Fig. 5 shows the model–experiment comparison for RHF in opt. ZIRLO. In contrast to Zircaloy-4, opt. ZIRLO exhibits a lower propensity for hydride reorientation. This behavior is captured in the model through a single alloy-dependent parameter controlling the sensitivity of hydride reorientation to applied stresses ($\Delta\Omega$ in Eq. (3)). The calculated mean absolute error (both alloys) for RHF is 0.04.

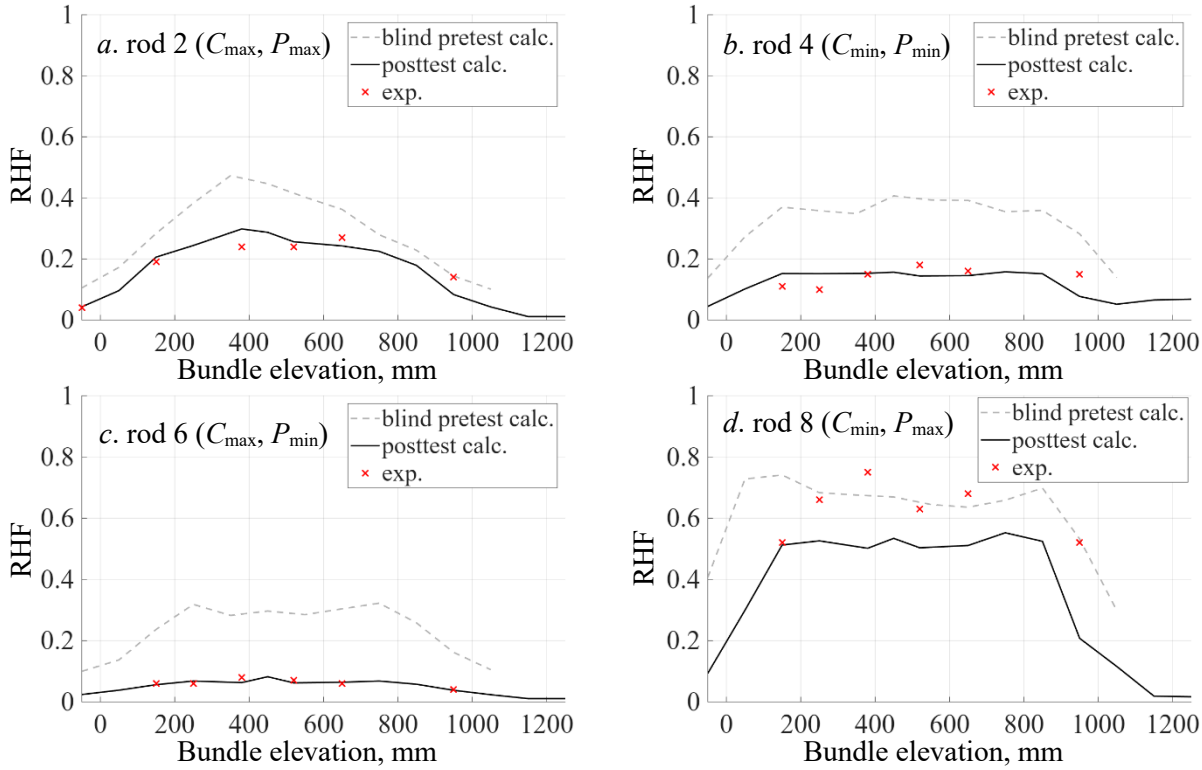

Figure 4. RHF in Zircaloy-4, model-experiment comparison; C_{max}/C_{min} corresponds to 300/100 ppm, (target concentration), P_{max}/P_{min} corresponds to 146/106 bar (target internal pressure)

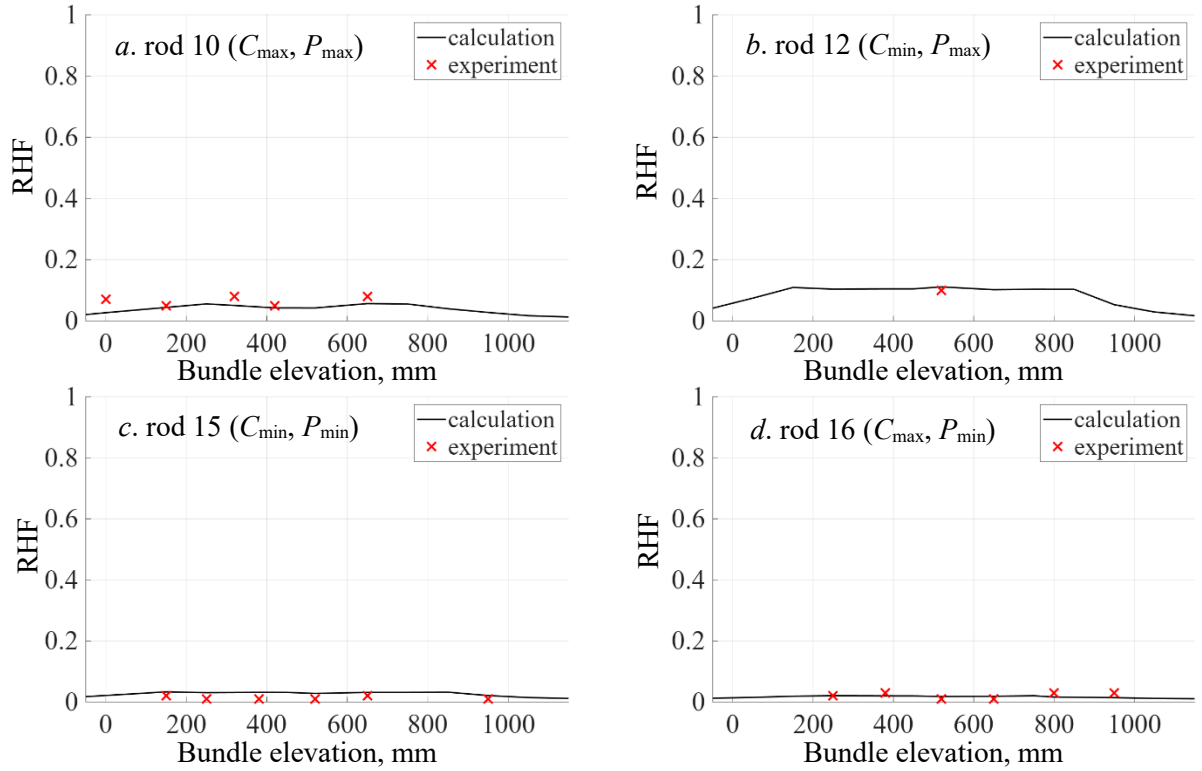

Figure 5. RHF in opt. ZIRLO, model-experiment comparison; C_{max}/C_{min} corresponds to 300/100 ppm, (target concentration), P_{max}/P_{min} corresponds to 146/106 bar (target internal pressure)

Figs. 6 and 7 compare the mean hydride length and hydride surface density for Zircaloy-4 and opt. ZIRLO. The simulated and experimentally measured values may differ by up to a factor of two, which is considered acceptable at the current stage of tool development. The calculated relative RMSE values for hydride length and hydride density are 25% and 20%, respectively. Hydride length and density are governed by the balance between the nucleation rate and the supersaturation relaxation rate and are therefore highly sensitive to uncertainties in key model parameters, including hydrogen solubility, hydrogen content, and defect-related energies. The present results were obtained using a smoothed temperature scenario (Fig. 3*b*). Compared to Zircaloy-4, opt. ZIRLO exhibits longer hydrides and a lower hydride surface density. This alloy-dependent behavior is captured in the model by assuming different densities of nucleation sites (n_0 in Eq. (4)), which may be associated with differences in crystallographic texture and in the density of high-energy grain boundaries with large misorientations.

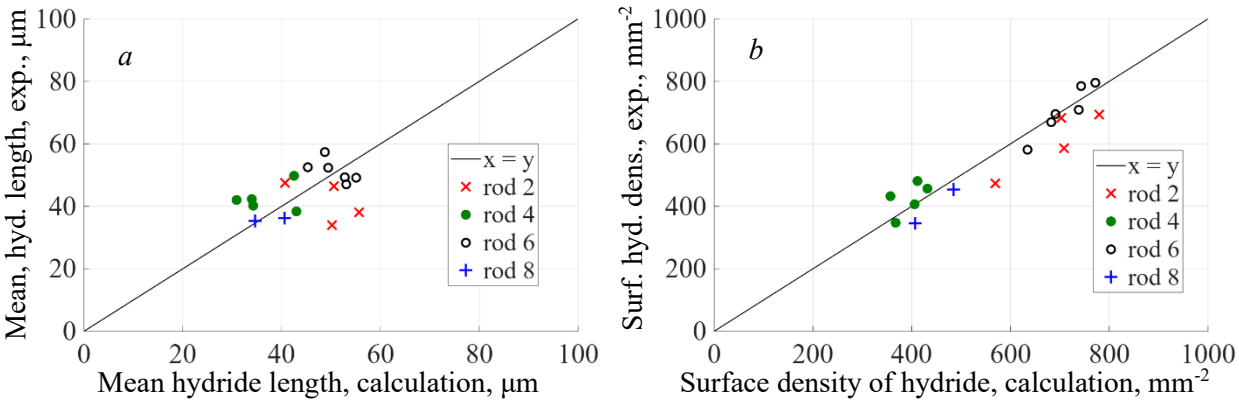

Figure 6. Experiment vs. calculation comparison in Zircaloy-4; *a*) mean hydride length, *b*) surface density of hydrides (number of hydrides per unit area on the micrograph)

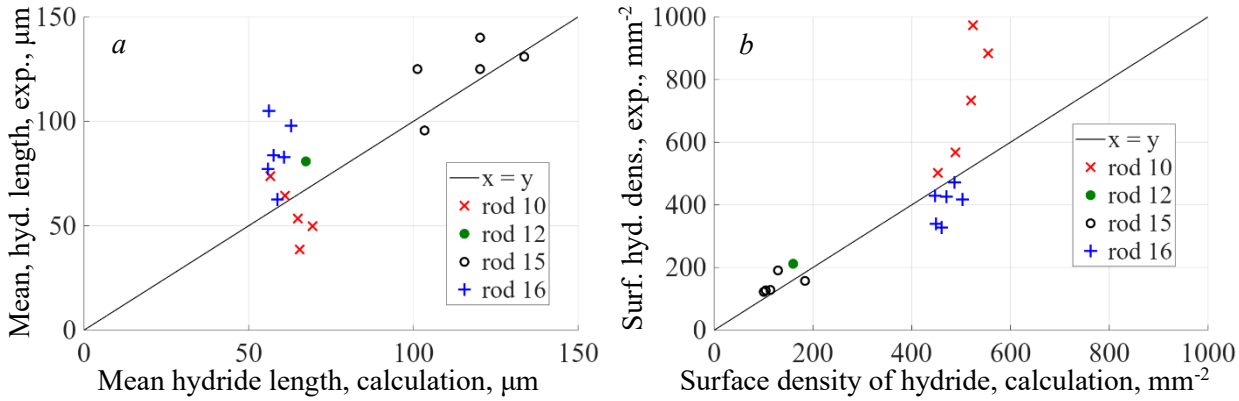

Figure 7. Experiment vs. calculation comparison in opt. ZIRLO; *a*) mean hydride length, *b*) surface density of hydrides (number of hydrides per unit area on the micrograph)

4. MORPHYD SIMULATION TOOL

4.1. The description of the tool

The numerical tool MORPHYD (an acronym of MORPHology of HYDrides), described in [15], [16], is another approach used to simulate the morphology of hydrides under the conditions of the SPIZWURZ bundle test. The physical basis of MORPHYD is very similar to the model described above; however, the

numerical realization is different. The fundamental difference is that MORPHYD simulates the nucleation and growth of disc-shaped hydrides in a virtual 3D domain. Nucleation occurs at uniformly distributed nucleation sites (defects in the crystal lattice) with a probability at the current time step τ equal to $r \cdot \tau$, where $r = R/n_0$ and R is given by Eq. (4). The orientation of the nucleated hydride is the stochastic value: the probability for radial orientation is f_r, and for circumferential orientation is $(1 - f_r)$, where f_r is determined by the Eq. (3). The growth of hydrides is determined by the diffusive flow from the solid solution to the end of the edge of the disk-shaped hydride [15], [17]. Another assumption is that each hydride can only absorb hydrogen from the space where it is the nearest hydride (in its Voronoi cell) [16]. This assumption takes into account the "clustering effect", i.e. that randomly closely related hydrides are expected to be shorter, than isolated ones due to "competition" for the hydrogen in the solid solution, needed for their growth during cooling.

Fig. 8*a* shows the MORPHYD simulation result for the hydride morphology in rod 4 at an elevation of 520 mm. Fig. 8*b* presents a cross-section of the simulated domain shown in Fig. 8*a*, which can be directly analyzed by analogy with the corresponding experimental micrographs. All MORPHYD simulation results are stochastic in nature. By repeating the simulations a statistically significant number of times, the statistical distributions of hydride morphology parameters can be evaluated using a Monte Carlo approach.

At its current stage of development, the model is limited to the simulation of the precipitation phase and is applicable only to small, non-overlapping hydrides, whose characteristic size remains smaller than the inter-hydride spacing. Consequently, MORPHYD was applied exclusively to samples with a hydrogen content of 100 ppm.

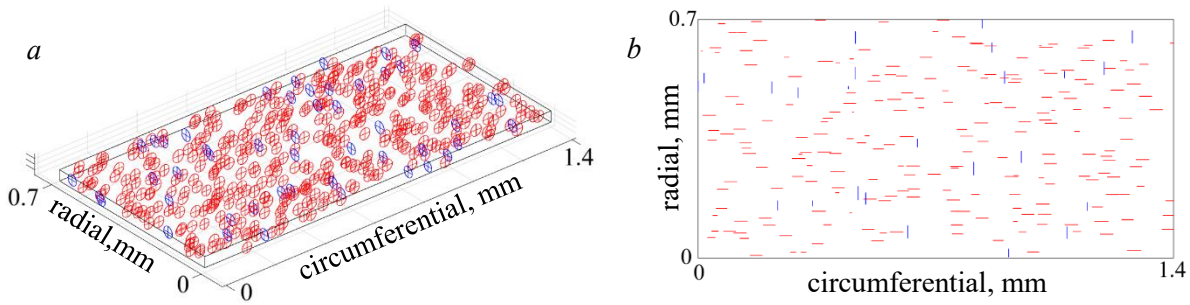

Figure 8: A single MORPHYD simulation result for rod 4 at 520 mm: *a*) disk-shaped hydrides with two orientations in a 3D domain; *b*) cross-section of the domain used for morphology analysis

4.1. Calibration and assessment of the MORPHYD

The following metrics were simulated with MORPHHYD and compared with experimental data: hydride length, hydride continuity coefficient (HCC, the sum of hydride length projected in radial direction in a 110 μm wide band, [6]) and radial hydride continuity path (RHCP, estimated as the relative reduction in calculated fracture energy for a given morphology compared to the samples without hydrides [6], [18]). By repeating the simulations at least 100 times, the statistical distribution of these morphology metrics can be estimated based on the Monte Carlo method. The calculated probability density functions (PDF) for the hydride morphology metrics in rods 4, 8, 12 and 15 at elevation 520 mm (the hottest axial zone) are compared with the experimental results on Figs. 9 – 11.

As shown in Fig. 9, the mean value and the width of the hydride length distributions obtained from simulations are in good agreement with the experimental data for both Zircaloy-4 and opt. ZIRLO. A notable

deviation is observed for rod 12, for which the simulated mean and distribution width are approximately a factor of two lower than the experimental values. Nevertheless, this discrepancy is considered acceptable at the current stage of tool development. In both experiments and simulations, the hydride length distributions are well described by a lognormal function characterized by a long-length tail [11]. In the simulations, this tail arises from the merging of several neighboring hydrides located at mutual distances smaller than approximately 5 μm, which are represented as a single elongated hydride.

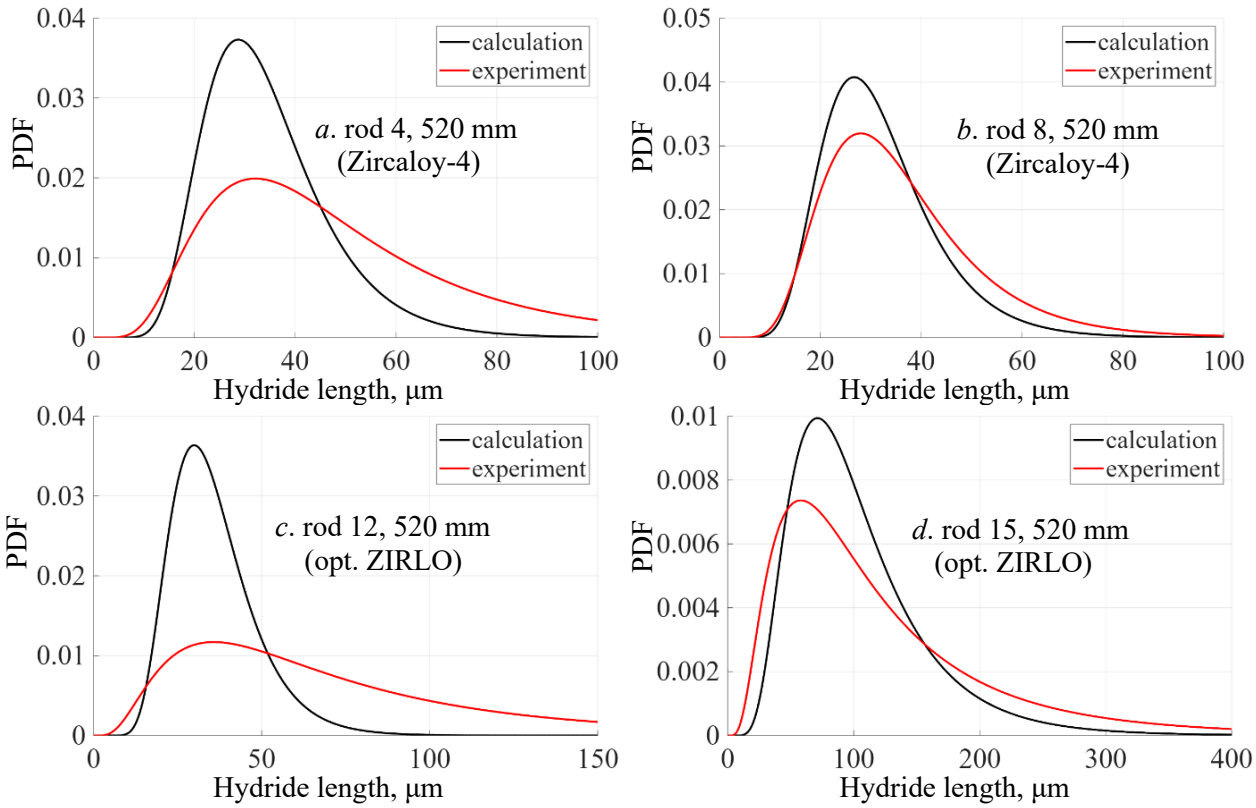

Figure 9. Statistical distributions of hydride lengths: comparison of experiment and calculation;

The calculated statistical distributions of the HCC and the RHCP are shown in Figs. 10 and 11, respectively. These distributions are compared with the corresponding experimental values obtained for the same cross-sections, which are indicated by dotted lines. The experimental HCC values are systematically higher than the mean values of the simulated distributions, whereas the experimental RHCP values are consistently lower than the corresponding simulated means. Nevertheless, when the finite width of the simulated distributions is taken into account, the experimental values remain comparable to the calculated results. The experimental value lies within the central 90% interval of the simulated distribution. Overall, the agreement between simulations and experiments is considered acceptable at the current stage of model development. Both HCC and RHCP exhibit the correct qualitative trends with increasing internal pressure and attain physically reasonable absolute values.

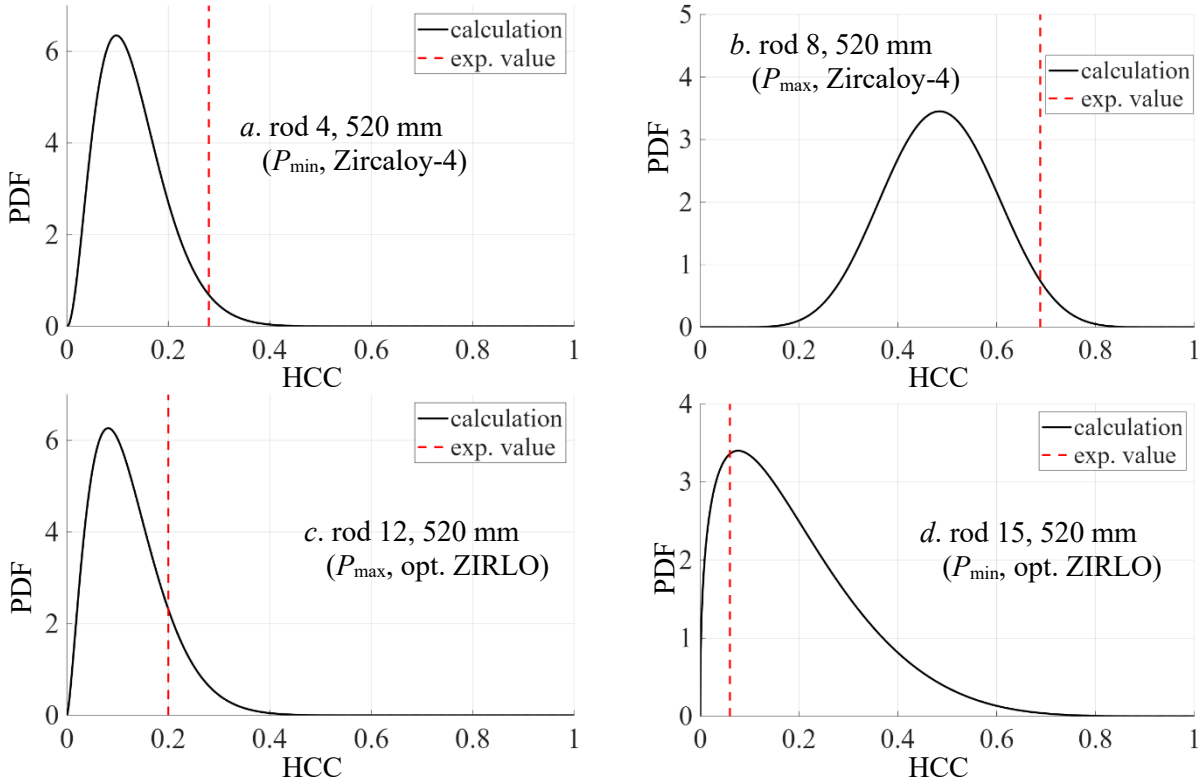

Figure 10. Calculated statistical distributions of HCC, compared with a single measurement

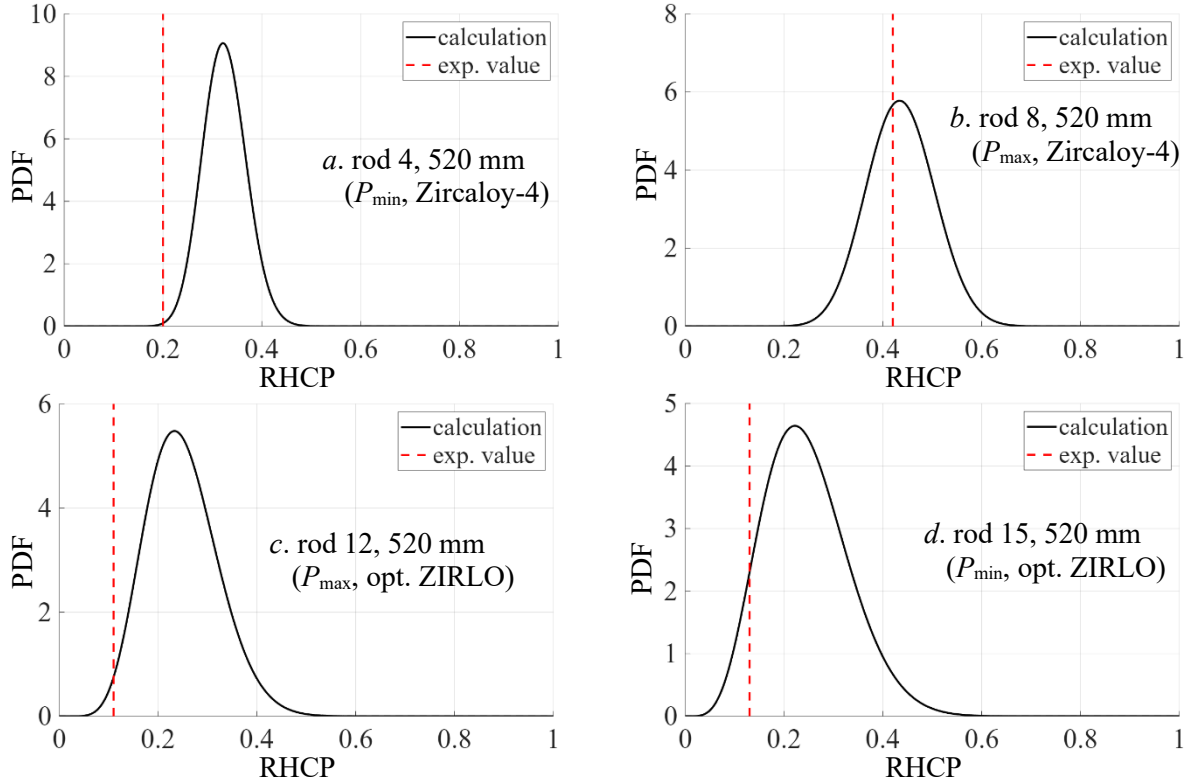

Figure 11. Calculated statistical distributions of RHCP, compared with a single measurement

5. CONCLUSION

Two numerical tools developed for the simulation of hydride morphology in zirconium alloys have been calibrated using new experimental data for Zircaloy-4 and opt. ZIRLO obtained in the SPIZWURZ test. Both numerical tools are complementary and can be used in tandem for advanced simulations.

The tool, based on the solution of the ODE system, is able to simulate the mean values of RHF, hydride length and density. The mean absolute error for RHF is 0.04, while the relative RMSE values for hydride length and density are 25% and 20%, respectively. A more systematic sensitivity analysis with respect to thermal-history assumptions and selected model parameters, including calculations with non-smoothed temperature histories, will be reported separately.

The MORPHYD tool showed the satisfactory agreement of the statistical distributions of hydride length, HCC and RHCP. The current limitations of MORPHYD are related to its precipitation stage only, the simplified description of hydride growth, and the restriction to small, non-overlapping hydrides. Therefore, the present MORPHYD assessment is limited to the 100 wppm cases.

ACKNOWLEDGMENTS

The SPIZWURZ project (FKZ RS1586A/1501609B) is funded by the Federal Ministry for the Environment, Nature Conservation, Nuclear Safety and Consumer Protection (BMUV).

REFERENCES

[1] A.T. Motta *et al.*, "Hydrogen in zirconium alloys: A review," *J. Nucl. Mater.*, **518**, pp. 440–460 (2019), DOI: 10.1016/j.jnucmat.2019.02.042.
[2] S. Suman *et al*., "Hydrogen in Zircaloy: Mechanism and its impacts," *Int. J. Hydrogen Energy*, **40** (17), pp. 5976–5994 (2015), DOI: 10.1016/j.ijhydene.2015.03.049.
[3] M. Kolesnik, "Micro-mechanisms of the ductile-to-brittle transition in hydrogenated zirconium alloys: A review and a comparison analysis of experimental data and theoretical approaches," *Eng. Fail. Anal.*, **159**, p. 108110 (2024), DOI: 10.1016/j.engfailanal.2024.108110.
[4] Q. Fang, M.R. Daymond, and A. King, "Study on the morphology of bulk hydrides by synchrotron X-ray tomography," *Mater. Charact.*, **134**, pp. 362–369 (2017), DOI: 10.1016/j.matchar.2017.11.013.
[5] M. Meyer *et al.*, "3D Hydrides Arrangement in Fuel Cladding Tubes and Timely Development of Hydrogen Relocation in Liner Cladding Investigated with Neutron Imaging," *Proceedings of TopFue 2024 reactor fuel performance conference*, Grenoble, France, 20 Sept. – 3 Oct. 2024, pp. 68–78 (2024).
[6] P.C.A. Simon *et al.* "Quantifying the effect of hydride microstructure on zirconium alloys embrittlement using image analysis," *J. Nucl. Mater.*, **547**, p. 152817 (2021), DOI: 10.1016/j.jnucmat.2021.152817.
[7] D. Hardie and M. W. Shanahan, "Stress reorientation of hydrides in zirconium-2.5% niobium," *J. Nucl. Mater.*, **55** (1), pp. 1–13 (1975), DOI: 10.1016/0022-3115(75)90132-4.
[8] M. Kolesnik, "Comparison of two kinetic approaches for modeling of radial hydride fraction in zirconium-based fuel rod cladding," *Nucl. Eng. Technol.*, 57**,** p. 103479 (2025), DOI: 10.1016/j.net.2025.103479.
[9] S.J. Min, M.S. Kim, and K.T. Kim, "Cooling rate- and hydrogen content-dependent hydride reorientation and mechanical property degradation of Zr-Nb alloy claddings," *J. Nucl. Mater.*, **441** (1-3), pp. 306–314 (2013), DOI: 10.1016/j.jnucmat.2013.06.006.
[10] M. Grosse *et al.*, "The SPIZWURZ project – Experimental investigations and modeling of the behavior of hydrogen in zirconium alloys under long-term dry storage conditions," *Nucl. Eng. Technol.*,. **56**, pp. 824–831 (2024), DOI: 10.1016/j.net.2023.09.027.
[11] M. Kolesnik, J. Stuckert, M. Grosse, and S. Weick, "Hydride morphology in zirconium cladding tubes after the SPIZWURZ bundle test . Part I : analysis of experimental data," *J. Nucl. Mater.*, **619**,

p. 156250 (2026), DOI: 10.1016/j.jnucmat.2025.156250.
[12] M. Kolesnik, T. Aliev, and V. Likhanskii, "Modeling of size, aspect ratio, and orientation of flattened precipitates in the context of Zr-H system under external stress," *Comput. Mater. Sci.*, **189**, p. 110260 (2021), DOI: 10.1016/j.commatsci.2020.110260.
[13] A.R. Massih and L.O. Jernkvist, "Stress orientation of second-phase in alloys: Hydrides in zirconium alloys," *Comput. Mater. Sci.*, **46** (4), pp. 1091–1097 (2009), DOI: 10.1016/j.commatsci.2009.05.025.
[14] Y.J. Kim, D.H. Kook, T.H. Kim, and J.S. Kim, "Stress and temperature-dependent hydride reorientation of Zircaloy-4 cladding and its effect on the ductility degradation," *J. Nucl. Sci. Technol.*, **52** (5), pp. 717–727 (2014), DOI: 10.1080/00223131.2014.978829.
[15] M. Kolesnik and T. Aliev, "Evaluating the spatial and size distributions of flat precipitates in diffusion-controlled precipitation processes," *Phys. Met. Metallogr.*, **104**, pp. 1414–1425 (2023), DOI: 10.1134/S0031918X22602074.
[16] T. Aliev and M. Kolesnik, "Evolution of an approach to the modeling of zirconium hydrides morphology based on Monte-Carlo method in 3D representation," *Lett. Mater.*, **13** (2), pp. 143–148 (2023), DOI: 10.22226/2410-3535-2023-2-143-148.
[17] T. Aliev and M. Kolesnik, "Stress concentrator at the plate-like inclusion tip as an enhancement factor of diffusion flux," *J. Phys. Commun.*, **5** (10), p. 105005 (2021), DOI: 10.1088/2399-6528/ac2a97.
[18] D. Kim, D. Kim, D. Woo, and Y. Lee, "Development of an image analysis code for hydrided Zircaloy using Dijkstra's algorithm and sensitivity analysis of radial hydride continuous path," *J. Nucl. Mater.*, **564**, p. 153647 (2022), DOI: 10.1016/j.jnucmat.2022.153647.
[19] J.J. Kearns, "Diffusion coefficient of Hydrogen in alpha Zirconium, Zircaloy-2 and Zircaloy-4," *J. Nucl. Mater.*, **43** (3), pp. 330–338 (1972), DOI: 10.1016/0022-3115(72)90065-7.
[20] J.S. Kim and Y.S. Kim, "Effect of thermal history on the terminal solid solubility of hydrogen in Zircaloy-4," *Int. J. Hydrogen Energy*, **39** (29), pp. 16442–16449 (2014), DOI: 10.1016/j.ijhydene.2014.08.018.
[21] J.S. Kim, T.H. Kim, K. Kim, and Y.S. Kim, "Terminal solid solubility of hydrogen of optimized-Zirlo and its effects on hydride reorientation mechanisms under dry storage conditions," *Nucl. Eng. Technol.*, **52** (8), pp. 1742–1748 (2020), DOI: 10.1016/j.net.2020.01.022.

APPENDIX A

Table I. Model parameters used in simulations

Alloy	Param.	Desciption	Value	Ref.
Both	D_{H}	Diffusion coefficient	$7 \times 10^{-7} \cdot \exp(-5360/T)$ [m^2/s]	[19]
	γ	hydride surface energy	0.065 [J/m^2]	[12, 13]
	v_{H}	atomic volume of H	1.7×10^{-29} [m^3]	[12]
	f_0	reorient param. from Eq. (3)	700	–
	E_{d0}	mean and standard deviation	9.6×10^{-19} [J]	–
	$\bar{\sigma}$	of defect energy norm. distr.	1.9×10^{-19} [J]	–
Zircaloy-4	C_{eq}^{TSSD}	solubility for dissolution	$2.255 \times 10^{5} \cdot \exp(-39101/RT)$ [wppm]	[20]
	C_{eq}^{TSSP}	solubility for precipitation	$8.612 \times 10^{4} \cdot \exp(-30583/RT)$ [wppm]	[20]
	n_0	nucleation site dens.	1×10^{15} [m^{-3}]	–
	$\Delta\Omega$	reorient param. from Eq. (3)	4.93×10^{-28} [m^{-3}]	–
opt. ZIRLO	C_{eq}^{TSSD}	solubility for dissolution	$7.8029 \times 10^{4} \cdot \exp(-35620/RT)$ [wppm]	[21]
	C_{eq}^{TSSP}	solubility for precipitation	$1.3256 \times 10^{5} \cdot \exp(-32824/RT)$ [wppm]	[21]
	n_0	nucleation site dens.	2×10^{14} [m^{-3}]	–
	$\Delta\Omega$	reorient param. from Eq. (3)	3.23×10^{-28} [m^{-3}]	–